Applied Energy 301 (2021) 117460

Contents lists available at ScienceDirect

Applied Energy

journal homepage: www.elsevier.com/locate/apenergy

Network-secure bidding optimization of aggregators of multi-energy systems in electricity, gas, and carbon markets

António Coelho [a,*], José Iria [b], Filipe Soares [a]

[a] Centre for Power and Energy Systems, INESC TEC, 4200-465 Porto, Portugal
[b] College of Engineering & Computer Science, Australian National University, Canberra, Australia

HIGHLIGHTS

- Distributed bidding strategy for aggregators of multi-energy systems in electricity, gas, and carbon markets.
- Distributed approach based on the alternating direction method of multipliers.
- The strategy computes multi-energy and network-secure bids from the electricity, gas, and heat operators' perspectives.

ARTICLE INFO

Keywords:
Aggregator
ADMM
CO2 markets
Day-ahead energy markets
Multi-energy systems
Secondary reserve market

ABSTRACT

The increasing replacement of conventional generators by variable renewable energy sources is reducing the flexibility of the power system, and consequently reducing its reliability indexes. To compensate for this reduction of flexibility, market participation of aggregators of multi-energy systems has been proposed in the literature. Under this scope, this paper presents a network-secure bidding optimization strategy to assist aggregators of multi-energy systems calculating electricity (energy and reserve), gas and carbon bids, considering multi-energy network constraints. This strategy is a distributed approach based on the alternating direction method of multipliers, where the aggregator collaborates with the operators of electricity, gas and heat networks to calculate network-secure bids. The proposed strategy is benchmarked against two other approaches. The results show that the newly developed strategy computes multi-energy and network-secure bids with execution times that suit the timelines of the electricity, gas, and carbon markets. The joint optimization of multi-energy systems reduced the aggregator's costs by 89% compared to a single energy-vector approach. Furthermore, two sensibility studies were also performed. The first study revealed that in the presence of slow ramp-rate resources (e.g. combined heat and power systems), aggregator's costs can decrease up to 87% when considering slower response times to the secondary reserve signal. In the second study, it was observed that the bidding behavior of the aggregator only starts changing significantly with carbon prices higher than 200€/tCO2.

1. Introduction

1.1. Motivation and aim

To achieve the goal of the Paris Agreement of keeping the rise of global temperature lower than 2 °C [1], the European Union (EU) has set its own goals to reduce CO2 emissions by at least 55% by 2030 [2]. The measures to adopt are mainly focused on the integration of renewable energy sources (RES), energy efficiency and the implementation of an EU emission trading system (ETS), generally known as the EU carbon market. The EU ETS is seen as "the cornerstone of the Union's climate policy" and it is the main instrument to achieve the emissions reduction target [3]. It is currently in its 4th phase which, compared to the previous phases, will be more demanding to participants as they will have more pressure to reduce emissions.

On the other hand, the decarbonization of the energy system by using RES has been ongoing for several years. Despite the benefits they bring, it is now proven that they are increasing the uncertainty and may jeopardizing the secure operation of the energy system due to their variability. To counteract this, new strategies are being developed like using prosumers' flexibility through demand response programs that are managed by aggregators or using multi-energy systems as they can provide more flexibility due to the possibility to optimize different

* Corresponding author.
E-mail address: antonio.m.coelho@inesctec.pt (A. Coelho).

https://doi.org/10.1016/j.apenergy.2021.117460
Received 26 March 2021; Received in revised form 2 July 2021; Accepted 16 July 2021
Available online 28 July 2021
0306-2619/© 2021 Elsevier Ltd. All rights reserved.

Nomenclature

Indices and sets

$d \in \{E, G, H\}$	Energy vectors (E: electricity, G: gas, H: heat)
$j \in J$	Clients
$J_n \subset J$	Clients per bus n
k	ADMM iteration
$m, n, i \in N^E, N^G, N^H$	Buses/nodes of electricity, gas, and heat networks
$(m, n), (\mathrm{j}, \mathrm{i}) \in B^E, B^G, B^H$	Lines/pipelines from bus m to bus n for electricity, gas, and heat networks
$s \in \{E, U, D\}$	Energy scenarios (En: energy, U: upward, D: downward)
$t, y \in T$	Time intervals
$v \in \{\mathrm{E}, \mathrm{G}, \mathrm{C}\}$	Markets (E: electricity, C: carbon, G: gas)

Superscripts

Abs	Absolute tolerance
Amb	Ambient temperature of pipelines' surrounding
AGC	Automatic generation control
B	Electricity reserve band bid
C	Carbon market
CFA	Free allowances of carbon market
CHP	Combined heat and power
CO2	Carbon dioxide
D	Downward reserve
DA	Day-ahead
DH	District heating
Dual	Dual residual
E	Electricity
EH	Heat pump
En	Energy
End	End of pipeline
F	Power flow
G	Gas
H	Heat
IL	Inflexible load
In	Input flow
O	Outdoor temperature
Ot	Outlet temperature
Out	Output flow
Primal	Primal residual
PV	Photovoltaic system
S	Supply temperature
Start	Start of pipeline
Sto	Storage system
U	Upward reserve
+,−	Charging, discharging of electric storage systems or positive, negative
¯, _	Maximum, minimum
∧	DSOs replicated values

Parameters

c	Factor to convert kWh to m^3/h
CP	Specific heat of water (kWh/°C)
FA	Free allowances (tCO2)
h	Heat transfer coefficient (W/°C)
k	Coefficient of pressure loss in water pipelines
K	Value of gas well coefficient
L	Length of the pipeline (m)
r	Resistance of power lines (p.u.)
R	Resistance of thermal buildings (°C/kW)
SB	Base power (kVA)
x	Reactance of power lines (p.u.)
Δt	Length of the time interval t (h)
λ	Price (€/kWh, €/kW or €/tCO2)
ϕ	Ratio
ϑ	Heat gains and losses not modeled explicitly (°C)
β	Thermal constant
η	Efficiency/coefficient of performance
ρ	Penalty of the augmented Lagrangian (€/kW^2)
α	Parameter that converts kWh of natural gas to tonnes of CO2
μ	Parameter of response of CHPs
ϵ	Residual tolerance

Variables

A	Number of allowances (tCO2)
b	Binary variable
D	Downward band bid (kW)
E	Energy bid (kWh)
ℓ	Square of the current magnitude (p.u.)
m	Mass flow of pipelines (kg/s)
mq	Mass flows of heat loads and generators (kg/s)
p	Pressure (gas: bar, heat: Pa)
P	Power (kW)
q	Gas flows (m^3/h)
Q	Reactive power (p.u.)
SOC	State-of-charge (kWh)
U	Upward band bid power (kW)
v	Square of the voltage magnitude (p.u.)
X	Internal variables of the aggregator problem
Y	Internal variables of the energy DSO problem
θ	Temperature (°C)
φ	Auxiliary binary variable
π	Dual variables of the augmented Lagrangian (€/kW)

energy networks or energy sources. However, these new measures and strategies also pose new challenges to aggregators and network operators related to network technical problems, data privacy, independence of roles and computational complexity.

Following this motivation, we propose an approach that addresses the new challenges identified in this section and fills the gaps found in the literature, as exposed in section 1.2.

1.2. Literature review

To study the benefits of multi-energy systems, some works considered the operational interactions and constraints between different distributed multi-energy resources (DMER) and networks. These works usually consider a combination of electricity, gas and heat networks. In [4–6], the constraints between electricity and gas networks were considered, in [7–9] between the electricity and heat networks and in [10–12] between the electricity, gas and heat networks. In these works, different optimization models to minimize operating costs or to improve the integration of RES, like wind, were developed.

All these works have one complex problem to solve which is related to the non-linear nature of modelling electricity, gas and heat networks. By performing a global optimization where the constraints of different resources, participants and networks are all considered together in the same problem, this may become very complex and difficult to solve. To counteract this, different strategies can be employed including the linearization of the individual networks or by developing new integrated models that can deal with the non-linear constraints. The linearization of the electricity networks is usually done by using a linear power flow

[4,6]. The linearization of the gas network can be done in different ways and in [4] was proposed a sequential linearization method, in [5] a sequential second-order cone programming linear approximation, in [6] an interval-based non-linear optimization and also in [13] a piece-wise linearization. The linearization of the district heating network can be done by considering different strategies like constant flow-variable temperature [9] or variable flow-constant temperature [14]. Concerning integrated models, it is often used an iterative Newton–Raphson method to solve the non-linear network problems [7,10–11] or other iterative [8] and genetic algorithms [12]. Nonetheless, this may not assure an optimal or feasible operation of the networks due to linearizations or inner approximations. For example, in the case of power systems, infeasible physical solutions may be generated in scenarios of low voltage as seen in [15,16].

To consider prosumers' flexibility and their participation in energy markets, the concept of an aggregator was created. The main purpose of aggregators is to optimize their clients' portfolio and participate in energy markets using bidding strategies. There is a diversified range of bidding strategies present in the literature. Some works developed deterministic models [17,18] while other developed stochastic models [19,20]; some developed models to participate solely in electrical energy markets [21] while others also considered secondary [18,19,22], tertiary [20] or other reserve markets [23,24]. Even though multiple studies oriented to multi-energy systems were performed, most of the existing publications focus on the technical operation of resources and energy networks and few studies were found that developed bidding models for multi-energy aggregators to participate in multi-energy markets. In [25–27], different models considering the capability to control multi-energy resources and the participation in electricity and gas markets were developed. In [28], a framework for a multi-energy virtual power plant to participate in electricity (energy and reserve) and hydrogen markets was developed. Nonetheless, the models in [25–27] did not consider the reserve markets, which may be the most profitable market for the multi-energy systems, and in [28] the gas market was not addressed. Furthermore, no studies were found in the literature that considered the participation of aggregators in carbon markets.

The bidding models presented in [17–21,25–27] are network-free since they do not consider the distribution network constraints in the calculation of the bids. These bidding models may compute network-infeasible bids in scenarios of high DMER integration [22,23], which might increase the cost of operating distribution networks since distribution system operators (DSO) may need to acquire services to solve possible voltage and congestion problems. Furthermore, the DSO may have to curtail aggregator's bids and its services are not delivered. In this scenario, the aggregator is penalized with fines or even forbidden to participate in the markets.

To increase the observability over distribution networks and counteract the network problems, several works developed centralized [24,28,29] and distributed strategies [22,23] to compute electricity network-secure bids. Centralized models solve the bidding and network problems together by using electricity DSO's network data. Under this scenario, the data privacy of the electricity DSO is not preserved. On the other hand, distributed strategies can solve the bidding and network problems separately. The model developed in [22] uses the alternating direction method of multipliers (ADMM) to compute network-secure bids in a distributed manner and preserve the data privacy of aggregators and the DSO. This approach also reduces the complexity of solving a large-scale problem by dividing it into smaller and less complex problems.

According to the gaps identified in this section, an integrated approach to support the participation of an aggregator in multi-energy markets (including electricity, gas and carbon markets) considering the non-linear constraints of electricity, gas and heat networks is still lacking in the literature. The following subsection describes the contributions of this work to fill in the identified gaps.

1.3. Contributions and advantages of the proposed model

This paper proposes an innovative strategy to assist an aggregator of multi-energy systems making optimal network-secure bidding decisions in several day-ahead markets. This bidding strategy minimizes the costs of the aggregator trading energy, gas and carbon allowances in the day-ahead electricity (energy and secondary reserve), gas, and carbon markets, while simultaneously ensures that the constraints of multi-energy networks (electricity, gas and heat) are not violated. The bidding strategy is a distributed approach based on the ADMM, where the aggregator interacts with the DSO of each energy vector (i.e., electricity, gas and heat) to compute multi-energy and network-secure bids. This negotiation allows the aggregator and DSOs to solve independently their bidding and network sub-problems, preserving the data privacy of all agents.

Given the above literature review, the main contributions of our bidding strategy are the following:

- It supports the participation of an aggregator of multi-energy systems in day-ahead electricity (energy and secondary reserve), gas, and carbon markets. To the best of our knowledge, this is the first work that addresses the participation of an aggregator in these three different markets;
- It computes multi-energy (electricity, gas, and CO2) bids considering the constraints of electricity, gas and heat networks. This decreases the risk of the aggregator violating the constraints of the multi-energy networks in real-time, reducing consequently possible energy imbalances and reserve shortages due to network violations;
- It exploits distributed optimization (i.e. ADMM) to preserve the independent roles of energy operators and the data privacy of the aggregator and networks' resources. In addition, it makes possible to solve a large-scale problem in a time-effective manner by decomposing the original problem into smaller sub-problems.

In addition to the contributions described above, the following sensibility studies were performed:

- The economic impact of considering different secondary reserve response times in the presence of resources with a slow ramp-rate was evaluated (e.g. combined heat and power (CHP));
- The influence of carbon prices on the performance of the aggregator was evaluated.

The effectiveness of the proposed bidding strategy was demonstrated in a real-world case study.

1.4. Paper organization

Section 2 describes the framework of the aggregator of multi-energy systems. Sections 3 and 4 describe the optimization sub-problems of the multi-energy aggregator and multi-energy DSOs. Sections 5 and 6 present the test case and the respective results. Finally, section 7 presents the conclusions of the work.

2. Framework for an aggregator of multi-energy systems

This section describes the framework for an aggregator of multi-energy systems. The framework includes the description of the aggregator's interactions with all the energy stakeholders (i.e., prosumers, market and network operators), as well as the decision-support tool required to enable the participation of the aggregator in the electricity, gas, and carbon markets.

2.1. Interactions of the aggregator with electricity, gas, and carbon markets

The aggregator of multi-energy systems participates in the day-ahead electricity, gas, and carbon markets of the Iberian Peninsula (Portugal and Spain). The electricity market includes energy and secondary reserve markets. The aggregator acts as a price-taker in these markets, by submitting demand (electricity), gas, and CO2 bids at cap-prices, and supply (electricity) and secondary reserve bids at floor-prices. This bidding behavior ensures that all the offers of the aggregator are accepted in the markets.

The energy session of the electricity market is a two-sided auction, where demand and supply bidders trade energy in the form of bids. The bids indicate the quantity (MWh) and price (€/MWh). The market operator collects the offers of all bidders and submits them to the European market-clearing platform (EUPHEMIA) to be dispatched [30]. The EUPHEMIA clears the bids such that the social welfare is maximized and the power flows between the European control areas do not exceed the capacity of the transmission interconnectors [31]. Afterwards, the transmission system operator (TSO) of each control area performs congestion management [32] to compute viable energy schedules, considering only the transmission network constraints of its area. In case of detected transmission network problems, the TSO can use market-based approaches (e.g., market-splitting) or technical-based methods (e.g., adjusting transformer taps) to solve the problems. In short, the EUPHEMIA and congestion management ensure that the energy bids do not violate any transmission network constraint between and within the European control areas.

The secondary reserve market begins after the congestion management phase. The TSO buys secondary reserve under the form of band (MW), taking into account the constraints of the transmission network of its control area [33]. Secondary reserve is remunerated under the form of availability (€/MW) and utilization (€/MWh). The price of band availability is set by the secondary reserve market, while the price of utilization is defined by the tertiary reserve market [21].

The energy session of the gas market is a daily trading auction. In this auction, the bidders can submit simple bids indicating the price (€/MWh) and daily quantity (MWh/day) of natural gas to be bought. The market operator gathers the bids and clears the market. The clearing price is calculated according to the point of intersection between the aggregated curves of supply and demand. Afterwards, the market agents inform the TSO about the quantity and direction of flow of gas to be deployed and the TSO validates them according to the technical constraints of the transmission gas network [34].

The EU carbon market (EU ETS) enables emitters of greenhouse emissions to buy allowances (in tonnes of CO2) to cover their yearly emissions. An emission allowance gives the right to emit a tonne of CO2. The market is a single-round, sealed bid and uniform price auction and occurs three times per week. In the market, the intermediaries of the installations (bidders) submit offers to buy a specific number of allowances at a given price (€/tCO2). Some installations receive free allowances (calculated through benchmarking [35]), such as CHP, due to the heat produced as a byproduct. Nonetheless, they still need to buy emission allowances to cover the CO2 emitted to generate electricity.

The chronological steps of the aggregator in the three markets are presented in Fig. 1, based on the current wholesale market rules. The first step of the aggregator is to compute the multi-energy bids, i.e., the electricity (energy and secondary reserve), gas, and CO2 bids. The second step of the aggregator is to submit the gas bids, before 9 h30. The third step is to submit the CO2 bids, before 11 h. The fourth step is to submit the energy bids, before 12 h. The final step is to submit the band bids to the secondary reserve market. This step only happens after the congestion management phase and the bids must be submitted before 19 h45.

2.2. Aggregator's interactions with electricity, gas, and heat DSOs

Today, the DSOs of electricity, gas, and heat do not participate directly in the wholesale markets as illustrated in Fig. 1. The current European rules do not allow the DSOs to participate, meaning that the network feasibility of the aggregator's offers is not checked by the DSOs.

In this paper, we propose that the aggregator negotiates with DSOs to compute multi-energy and network-secure offers, before the bids reach the wholesale markets. This additional step will allow the aggregator to fully deliver the services traded in the markets, avoiding high monetary fines for not delivering the services due to distribution network violations. Note that such violations can disconnect DMER from the network, and consequently blocking the aggregator from fully delivering the services traded in the wholesale markets. The aggregator could end up being expelled from the markets due to consecutive underperformance. Therefore, the energy system will benefit from the adoption of this new framework since more services will safely reach the wholesale markets from the DMER located in the distribution networks, reducing the energy costs and increasing the overall reliability of the energy system.

The negotiation strategy between the aggregator and DSOs is described in Section 2.2.1.

2.2.1. Multi-energy and network-secure bidding optimization strategy

The aggregator can compute network-secure bids by solving the optimization model (1)–(4). The objective function (1) minimizes the net cost of participating in the electricity, gas and carbon markets. Let X be the aggregator's internal variables and P^E, P^G, P^H be the power exchanged between the aggregator and each energy-vector DSO. Eq. (2) is the aggregator's constraints. Eq. (3) is the DSO's constraints, where $\widehat{P^d}$ is the duplicated variables of P^d, and Y^d is the internal variables of each DSO. Constraint (4) was added to the problem to enable the decomposition of the centralized problem into independent aggregator and DSOs sub-problems.

$$min\, f\left(P^E, P^G, P^H, X\right) \tag{1}$$

$$h\left(P^E, P^G, P^H, X\right) \leq 0 \tag{2}$$

$$g^d\left(\widehat{P}^d, Y^d\right) \leq 0, \forall d \in \{E, G, H\} \tag{3}$$

$$P^d - \widehat{P}^d = 0, \forall d \in \{E, G, H\} \tag{4}$$

We use ADMM to decompose the problem (1)–(4) into aggregators and DSOs sub-problems. This decomposition enables the aggregator and DSOs to solve their bidding and multi-energy network sub-problems independently without putting at risk the data privacy of each agent. In addition, the decomposition of (1)–(4) makes the problem easier to solve since it is divided into smaller and independent aggregator and DSOs sub-problems.

The bidding sub-problem of the aggregator is given by (5) and (6).

$$min\, f\left(P^E, P^G, P^H, X\right) + \sum_{d \in \{E,G,H\}} \mathscr{L}^d\left(P^d, \widehat{P}^{d,k}, \pi^{d,k}\right) \tag{5}$$

$$h\left(P^E, P^G, P^H, X\right) \leq 0 \tag{6}$$

The network sub-problem of each energy DSO d is given by (7) and (8).

$$\min \mathscr{L}^d\left(P^{d,k+1}, \widehat{P}^d, \pi^{d,k}\right) \tag{7}$$

$$g\left(\widehat{P}^d, Y^d\right) \leq 0 \tag{8}$$

Eq. (9) represents the penalty term of the augmented Lagrangian applied to constraint (4), where π is a vector with dual variables and ρ is a penalty scalar.

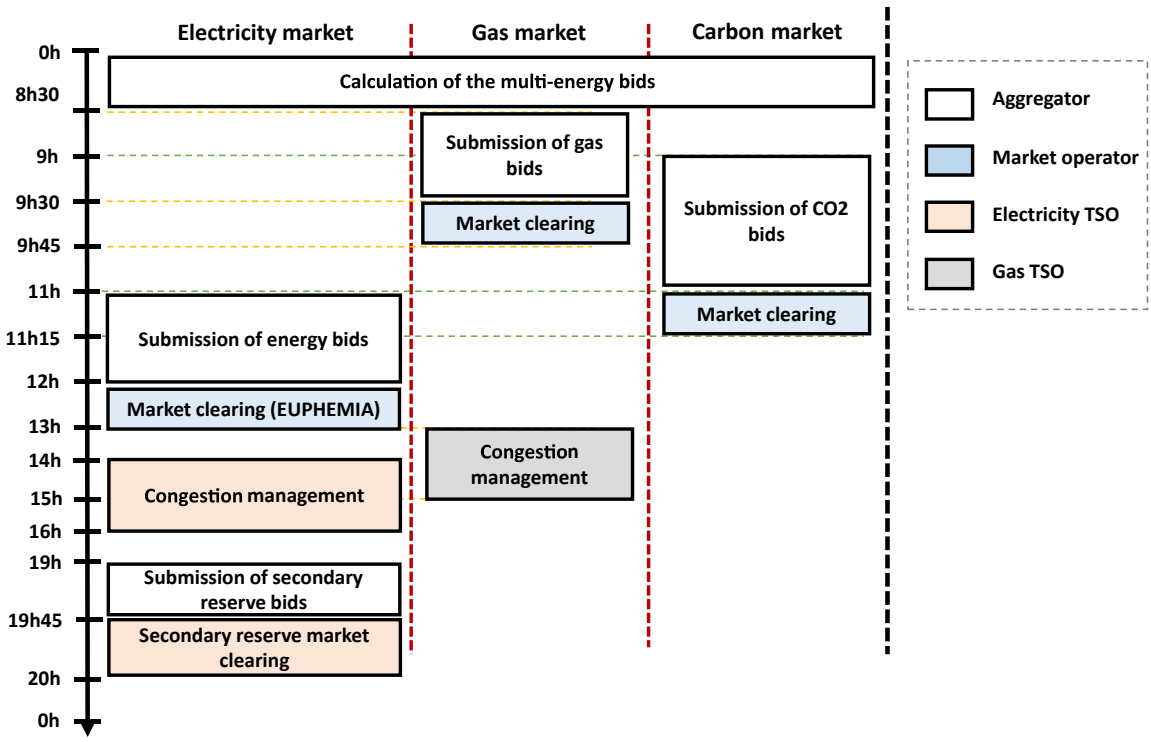

Fig. 1. Sequential steps of the aggregator in the electricity, gas, and carbon markets.

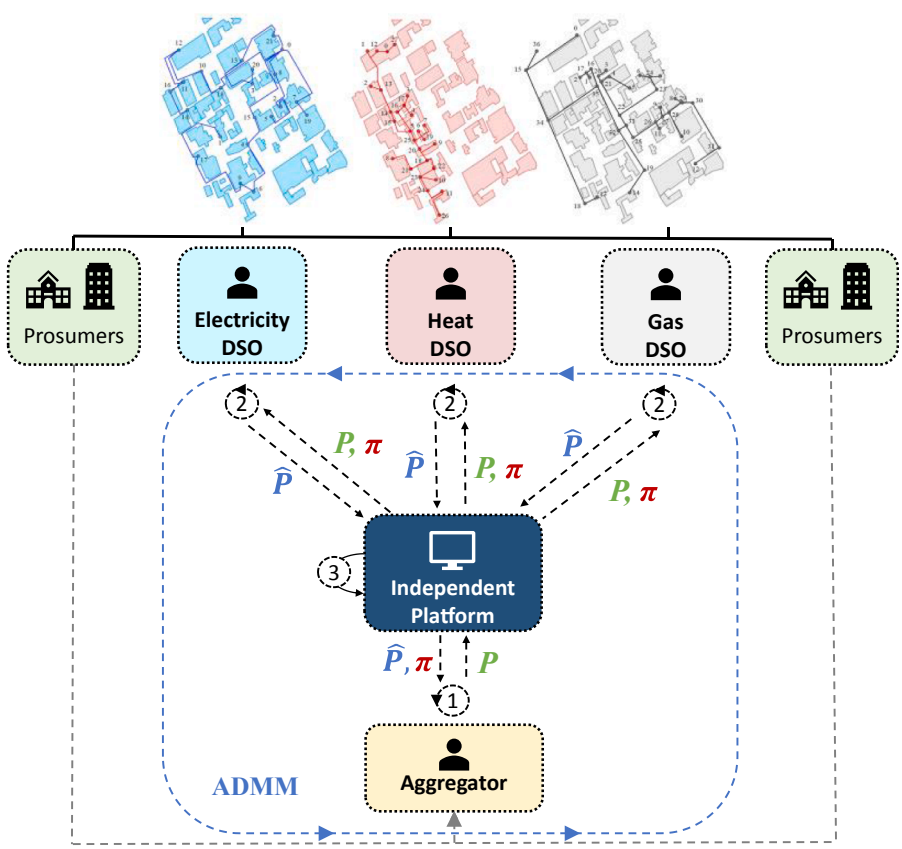

Fig. 2. ADMM algorithm.

$$\mathscr{L}^d\left(P^d,\widehat{P^d},\pi^d\right)=\pi^{d^{\mathrm{T}}}\left(P^d-\widehat{P^d}\right)+\frac{\rho}{2}\|P^d-\widehat{P^d}\|_2^2 \tag{9}$$

The ADMM algorithm solves the optimization problems (5)–(6) and (7)–(8) iteratively until convergence is reached. The steps of each iteration k of the ADMM are presented in Fig. 2 and described below:

1. The aggregator runs the optimization problem (5)–(6) and computes the bids by holding $\widehat{\boldsymbol{P}}^{d,k}$, $\boldsymbol{\pi}^{d,k}$ constant at $\boldsymbol{k^{th}}$ values. Values of $\boldsymbol{P^d}$ are obtained and communicated to the independent platform[1];
2. Each DSO runs its respective optimization problem from (7)–(8) and solves it by holding $\boldsymbol{P^{d,k+1}}$, $\boldsymbol{\pi^{d,k}}$ constant. Values of $\widehat{\boldsymbol{P}}^{\boldsymbol{d}}$ are obtained and communicated to the independent platform. The electricity DSO runs an AC optimal power flow and obtains the values of $\widehat{\boldsymbol{P}}^{\boldsymbol{E}}$; the gas DSO runs a non-linear steady state gas flow and obtains the values of $\widehat{\boldsymbol{P}}^{\boldsymbol{G}}$ and the heat DSO runs a non-linear heat flow and obtains the values of $\widehat{\boldsymbol{P}}^{\boldsymbol{H}}$.
3. An independent platform performs different actions. First, it updates the dual variables $\boldsymbol{\pi}$ using (10). Then, it checks for convergence with (11) and (12). If the convergence criteria are satisfied the algorithm stops, otherwise continues and updates ρ using a tuning strategy [37]. Finally, it communicates the updated dual variables and goes back to step 1.

Eq. (10) updates the dual variables π.

$$\pi^{d,k+1}=\pi^{d,k}+\rho\left(P^{d,k+1}-\widehat{P}^{d,k+1}\right) \tag{10}$$

The stop criteria are defined by Eqs. (11) and (12), where ϵ^{abs} is the absolute tolerance and a is the size of the primal and dual residuals as they are part of $\mathbb{R}^a$ [37]. Eq. (11) represents the violation of constraint (4). Eq. (12) represents the violation of the Karush-Kuhn-Tucker stationarity constraint.

$$\|\left(P^{d,k+1}-\widehat{P}^{d,k+1}\right)^T\|_2\leq\epsilon^{Abs}\sqrt{a} \tag{11}$$

$$\|\rho\left(\widehat{P}^{d,k+1}-P^{d,k+1}\right)^T\|_2\leq\epsilon^{Abs}\sqrt{a} \tag{12}$$

The network-secure bidding problem is formulated for a single aggregator but it can be extended to multiple aggregators without requiring any changes in the distributed formulation of the problem, as described in [22]. However, the aim of the paper is not to study the dynamics between multiple aggregators and DSOs, thus, and for sake of simplicity, it was decided to only consider a single aggregator.

2.3. Aggregator's interactions with prosumers

The aggregator exploits the flexibility of the multi-energy resources of the prosumers through demand response programs agreed upon a remuneration strategy, which is outside of the scope of this work. The DMERs include thermal loads, PV systems, energy storage systems (ESS), heat pumps (HP) and CHPs connected to the district heating network. The thermal loads and HPs are sources of demand flexibility; ESSs are sources of demand and generation flexibility; PV systems and CHPs are sources of generation flexibility. The prosumers also have electricity, gas and heat inflexible loads that have to be satisfied. It is assumed that aggregators communicate with the prosumers through a home energy management system, which encompasses a set of capabilities that grants control over DMERs [19].

3. Aggregator sub-problem: Bidding optimization model

This section presents the bidding optimization model (13)–(70) used by the aggregator to compute electricity (energy and secondary reserve), gas, and CO2 bids. In addition, the bidding model computes scenarios of operation for the electricity, gas and heat networks, i.e. bid delivery scenarios.

3.1. Objective function

The objective function (13) minimizes the net cost of the aggregator trading electricity, gas and CO2 in the day-ahead electricity (energy and secondary market), gas and carbon markets. The objective function (13) is divided into 4 terms. The first term (14) is the net cost of buying and selling energy and secondary reserve in the electricity markets. The second term (15) is the net cost of trading gas in the gas market. The third (16) and fourth (17) terms are the cost of buying CO2 allowances in the carbon market. These two terms penalize the CO2 emitted by the CHPs during the generation of electricity (16) and heat (17). The last term (18) is the penalty term of the augmented Lagrangian and penalizes violations in electricity, gas, and heat networks.

$$min\sum_{t\in T}\left[\sum_{v\in\{E,G,C\}}f_t^v+\sum_{d\in\{E,G,H\}}\sum_{s\in\{En,U,D\}}\sum_{n\in N^d}\mathscr{L}^d_{s,n,t}\right]+f^{CFA} \tag{13}$$

$$f_t^E=\lambda_t^E E_t^E\Delta t-\lambda_t^B(U_t^E+D_t^E)+\left(\lambda_t^{D,E}\phi_t^D D_t^E-\lambda_t^{U,E}\phi_t^U U_t^E\right)\Delta t \tag{14}$$

$$f_t^G=\lambda_t^G E_t^G\Delta t+\left(\lambda_t^{U,G}\phi_t^U U_t^G-\lambda_t^{D,G}\phi_t^D D_t^G\right)\Delta t \tag{15}$$

$$f_t^C=\lambda^{CO2}\sum_{j\in J_n}\left(P_{j,t}^{CHP,E}+U_{j,t}^{CHP,E}.\phi_t^U-D_{j,t}^{CHP,E}.\phi_t^D\right)\alpha^{CO2,G}\Delta t \tag{16}$$

$$f^{CFA}=\lambda^{CO2}.\mathrm{A}^{+,CO2} \tag{17}$$

$$\mathscr{L}^d_{s,n,t}=\pi^d_{s,n,t}\left(P^d_{s,n,t}-\widehat{P}^d_{s,n,t}\right)+\frac{\rho}{2}\left(P^d_{s,n,t}-\widehat{P}^d_{s,n,t}\right)^2 \tag{18}$$

3.2. Market constraints

Constraint (19) defines that the secondary reserve band must be 2/3 for upward and 1/3 for downward, according to the rules of secondary reserve market [19].

$$U_t^{DA}=2.D_t^{DA},\forall t\in T \tag{19}$$

Constraint (20) and (21) define the CO2 allowances that the aggregator has to buy due to the heat generated by the CHPs.

$$\mathrm{A}^{+,CO2}-\mathrm{A}^{-,CO2}=\sum_{t\in T}\sum_{j\in J_n}\left[\left(P_{j,t}^{CHP,H}+U_{j,t}^{CHP,H}.\phi_t^U-D_{j,t}^{CHP,H}.\phi_t^D\right).\alpha^{CO2,G}.\Delta t\right]-FA^{CO2} \tag{20}$$

$$\mathrm{A}^{+,CO2},\mathrm{A}^{-,CO2}\geq 0 \tag{21}$$

3.3. Bidding constraints

Constraints (22) and (23) define the electricity (demand and supply) and gas bids. Constraints (24) and (25) define the upward and downward secondary reserve bids. They include the flexibility provided by ESSs, PV systems, HPs and CHPs. Constraints (26) and (27) define gas imbalances generated due to the expected activation of secondary reserve provided by CHPs.

[1] An independent platform, managed by an authorized third-party entity, is used to preserve the data privacy of the aggregator and DSOs since the platform communicates to the aggregator and DSOs only the information that they require to solve their optimization sub-problems. It is worth mentioning that this third-party agent/platform also has been adopted by other researchers in similar contexts (e.g. [45]).

$$E_t^E = \sum_{n \in N^E} P_{n,t}^E, \forall t \in T \tag{22}$$

$$E_t^G = \sum_{n \in N^G} P_{n,t}^G, \forall t \in T \tag{23}$$

$$U_t^E = \sum_{j \in J_n} \left(U_{j,t}^{Sto} + U_{j,t}^{PV} + U_{j,t}^{EH} + U_{j,t}^{CHP,E} \right), \forall n \in N^E, t \in T \tag{24}$$

$$D_t^E = \sum_{j \in J_n} \left(D_{j,t}^{Sto} + D_{j,t}^{PV} + D_{j,t}^{EH} + D_{j,t}^{CHP,E} \right), \forall n \in N^E, t \in T \tag{25}$$

$$U_t^G = \sum_{j \in J_n} \left(U_{j,t}^{CHP,G} \right), \forall n \in N^G, t \in T \tag{26}$$

$$D_t^G = \sum_{j \in J_n} \left(D_{j,t}^{CHP,G} \right), \forall n \in N^G, t \in T \tag{27}$$

3.4. Delivery scenario constraints

Delivery scenarios define possible exchanges of power between aggregators' clients and energy networks. The DSOs use these scenarios to evaluate the network feasibility of aggregator's offers. The delivery scenarios are divided by energy vectors. The electricity scenarios include the delivery of energy (28), and the activation of upward (31) and downward (32) secondary reserves in real-time. The gas scenarios include the delivery of gas (29) and the gas imbalances (33)–(34) generated in real-time due to the activation of secondary reserve provided by CHPs. The heat scenarios include the delivery of heat (30) and the heat imbalances (35)–(36) generated in real-time due to the activation of secondary reserve provided by CHPs.

Constraint (28) defines the scenario of electricity delivery, which results from the sum of the electricity consumed by inflexible loads, HPs, ESSs and electricity generated by ESSs, PV systems and CHPs.

$$P_{n,t}^E = \sum_{j \in J_n} \left(P_{j,t}^{IL,E} + P_{j,t}^{EH} + P_{j,t}^{+} - P_{j,t}^{-} - P_{jt}^{PV} - P_{j,t}^{CHP,E} \right), \forall n \in N^E, t \in T \tag{28}$$

Constraint (29) defines the scenario of gas delivery, which results from the sum of the gas consumed by the inflexible loads and CHPs connected to the district heating.

$$P_{n,t}^G = \sum_{j \in J_n} \left(P_{j,t}^{IL,G} + P_{j,t}^{CHP,G} \right), \forall n \in N^G, t \in T \tag{29}$$

Constraint (30) defines the scenario of heat delivery, which results from the sum of the heat consumed by the inflexible and flexible heating loads connected to the district heating and the heat generated by CHPs.

$$P_{n,t}^H = \sum_{j \in J_n} \left(P_{j,t}^{IL,H} + P_{j,t}^{DH} - P_{j,t}^{CHP,H}. \right), \forall n \in N^H, t \in T \tag{30}$$

Constraint (31) defines the scenario of upward band activation in real-time. It considers the sum of the upward flexibility of HPs, ESSs, PV systems and CHPs. Constraint (32) defines the scenario of downward band activation in real-time. It considers the sum of the downward flexibility of HPs, ESSs, PV systems, and CHPs.

$$P_{n,t}^{U,E} = P_{n,t}^E - \sum_{j \in J_n} \left(U_{j,t}^{EH} + U_{j,t}^{Sto} + U_{j,t}^{PV} + U_{j,t}^{CHP,E} \right), \forall n \in N^E, t \in T \tag{31}$$

$$P_{n,t}^{D,E} = P_{n,t}^E + \sum_{j \in J_n} \left(D_{j,t}^{EH} + D_{j,t}^{Sto} + D_{j,t}^{PV} + D_{j,t}^{CHP,E} \right), \forall n \in N^E, t \in T \tag{32}$$

Constraints (33) and (34) define the scenarios of gas imbalances generated by the activation of upward and downward band reserves in real-time. The gas imbalances are defined in (26) and (27) results from the behavior of the CHPs.

$$P_{n,t}^{U,G} = P_{n,t}^G + \sum_{j \in J_n} \left(U_{j,t}^{CHP,G} \right), \forall n \in N^G, t \in T \tag{33}$$

$$P_{n,t}^{D,G} = P_{n,t}^G - \sum_{j \in J_n} \left(D_{j,t}^{CHP,G} \right), \forall n \in N^G, t \in T \tag{34}$$

Constraints (35) and (36) define the scenarios of heat imbalances generated by the activation of upward and downward band reserves in real-time. The heat imbalances result from the behavior of the district heating and CHPs.

$$P_{n,t}^{U,H} = P_{n,t}^H - \sum_{j \in J_n} \left(U_{j,t}^{DH} + U_{j,t}^{CHP,H} \right), \forall n \in N^H, t \in T \tag{35}$$

$$P_{n,t}^{D,H} = P_{n,t}^H - \sum_{j \in J_n} \left(D_{j,t}^{DH} + D_{j,t}^{CHP,H} \right), \forall n \in N^H, t \in T \tag{36}$$

3.5. DMER constraints

3.5.1. Heat pumps

The HPs are modelled by constraints (37)–(46). Constraint (37) defines the minimum and maximum limits. Constraints (38)–(40) define the limits of the upward and downward bands. Constraints (41)–(43) define the temperature in each delivery scenario (energy (28), upward (31) and downward (32) band activations). Constraints (44)–(46) model the comfort levels of the occupants.

$$\underline{P_{j,t}^{EH}} \le P_{j,t}^{EH} \le \overline{P_{j,t}^{EH}}, \forall j \in J, t \in T \tag{37}$$

$$U_{j,t}^{EH} \le P_{j,t}^{EH} - \underline{P_{j,t}^{EH}}, \forall j \in J, t \in T \tag{38}$$

$$D_{j,t}^{EH} \le \overline{P_{j,t}^{EH}} - P_{j,t}^{EH}, \forall j \in J, t \in T \tag{39}$$

$$D_{j,t}^{EH}, U_{j,t}^{EH} \ge 0, \forall j \in J, t \in T \tag{40}$$

$$\theta_{j,t+1}^{En} = \beta_j \theta_{j,t}^{En} + (1 - \beta_j) \left[\theta_{j,t}^O + R_j \left(\eta_j^{EH} P_{j,t}^{EH} \right) \right] + \vartheta_{j,t}, \forall j \in J, t \in T \tag{41}$$

$$\theta_{j,t+1}^{U} = \beta_j \theta_{j,t}^{U} + (1 - \beta_j) \left[\theta_{j,t}^O + R_j \left(\eta_j^{EH} P_{j,t}^{EH} - \eta_j^{EH} U_{j,t}^{EH} \right) \right] + \vartheta_{j,t}, \forall j \in J, t \in T \tag{42}$$

$$\theta_{j,t+1}^{D} = \beta_j \theta_{j,t}^{D} + (1 - \beta_j) \left[\theta_{j,t}^O + R_j \left(\eta_j^{EH} P_{j,t}^{EH} + \eta_j^{EH} D_{j,t}^{EH} \right) \right] + \vartheta_{j,t}, \forall j \in J, t \in T \tag{43}$$

$$\underline{\theta}_j \le \theta_{j,t+1}^{En} \le \overline{\theta}_j, \forall j \in J, t \in T \tag{44}$$

$$\underline{\theta}_j \le \theta_{j,t+1}^{U} \le \overline{\theta}_j, \forall j \in J, t \in T \tag{45}$$

$$\underline{\theta}_j \le \theta_{j,t+1}^{D} \le \overline{\theta}_j, \forall j \in J, t \in T \tag{46}$$

3.5.2. District heating flexible loads

The district heating flexible loads are modelled by the same constraints of the HPs (37)–(46). However, instead of modelling the electric power variables $\left\{ P_{j,t}^{EH}, D_{j,t}^{EH}, U_{j,t}^{EH} \right\}$, here we model the thermal variables $\left\{ P_{j,t}^{DH}, D_{j,t}^{DH}, U_{j,t}^{DH} \right\}$ in constraints (37)–(46).

3.5.3. PV systems

Constraint (47) defines the maximum power output of the PV system. The parameter $\overline{P_j^{PV}}$ is the forecasted generation. Constraints (48) and (49) define the band limits.

$$0 \le P_{j,t}^{PV} \le \overline{P_j^{PV}}, \forall j \in J, t \in T \tag{47}$$

$$0 \le U_{j,t}^{PV} \le \overline{P_j^{PV}} - P_{j,t}^{PV}, \forall j \in J, t \in T \tag{48}$$

$$0 \le D_{j,t}^{PV} \le P_{j,t}^{PV}, \forall j \in J, t \in T \tag{49}$$

3.5.4. Energy storage system constraints

The operation of the energy storage units is defined by constraints (50)–(60). Constraints (50) and (51) define the state-of-charge and its limits. Constraints (52) and (53) set the range of the charging and discharging power. Constraint (54) ensures that no simultaneous charging and discharging occurs. Constraint (55) ensures that the state-of-charge at the end of the day is equal to the initial state-of-charge.

$$SOC_{j,t+1} = SOC_{j,t} + \left(P_{j,t}^{+} \eta_j^{+} - \frac{P_{j,t}^{-}}{\eta_j^{-}} \right) \Delta t, \forall j \in J, t \in T \tag{50}$$

$$\underline{SOC_j} \le SOC_{j,t+1} \le \overline{SOC_j}, \forall j \in J, t \in T \tag{51}$$

$$0 \le P_{j,t}^{-} \le b_{j,t}^{-} . \overline{P_j^{Sto}}, \forall j \in J, t \in T \tag{52}$$

$$0 \le P_{j,t}^{+} \le b_{j,t}^{+} . \overline{P_j^{Sto}}, \forall j \in J, t \in T \tag{53}$$

$$b_{j,t}^{-} + b_{j,t}^{+} = 1, \forall j \in J, t \in T \tag{54}$$

$$SOC_{j,0} = SOC_{j,-1}, \forall j \in J \tag{55}$$

Constraints (56) and (57) limit the downward and upward bands. Constraints (58) and (59) guarantee that the storage only supply upward and downward bands if the state-of-charge is within the limits. Constraint (60) ensures that the storage has enough capacity to charge after providing upward or downward reserves [22].

$$0 \le D_{j,t}^{Sto} \le \overline{P_j^{Sto}} - P_{j,t}^{+}, \forall j \in J, t \in T \tag{56}$$

$$0 \le U_{j,t}^{Sto} \le \overline{P_j^{Sto}} - P_{j,t}^{-}, \forall j \in J, t \in T \tag{57}$$

$$U_{j,t}^{Sto}, D_{j,t}^{Sto} \le \frac{\overline{SOC_j} - SOC_{j,t+1}}{\eta_j \Delta t}, \forall j \in J, t \in T \tag{58}$$

$$U_{j,t}^{Sto}, D_{j,t}^{Sto} \le \frac{\left(SOC_{j,t+1} - \underline{SOC_j} \right) \eta_j}{\Delta t}, \forall j \in J, t \in T \tag{59}$$

$$\sum_{y \in T_t} \left(D_{j,y}^{Sto} + U_{j,y}^{Sto} \right) \le \sum_{y \in T_t} \left(\frac{\overline{P_j^{Sto}} - P_{j,y}^{+} - P_{j,y}^{-}}{2} \right), \forall j \in J, t \in T \tag{60}$$

3.5.5. District heating CHPs

Constraints (61)–(70) model the CHPs connected to the district heating. Constraint (61) sets the gas consumption range. Constraints (62) and (63) define the electricity and heat generated by the CHPs. Constraints (64)–(69) define the electricity, gas, and heat flexibilities of the CHPs to provide upward and downward reserve bands.

$$\underline{P_{j,t}^{CHP,G}} \le P_{j,t}^{CHP,G} \le \overline{P_{j,t}^{CHP,G}}, \forall j \in J, t \in T \tag{61}$$

$$P_{j,t}^{CHP,E} = \eta_j^{CHP,E} P_{j,t}^{CHP,G}, \forall j \in J, t \in T \tag{62}$$

$$P_{j,t}^{CHP,H} = \eta_j^{CHP,H} P_{j,t}^{CHP,G}, \forall j \in J, t \in T \tag{63}$$

$$0 \le U_{j,t}^{CHP,G} \le \overline{P_{j,t}^{CHP,G}} - P_{j,t}^{CHP,G}, \forall j \in J, t \in T \tag{64}$$

$$U_{j,t}^{CHP,E} = \eta_j^{CHP,E} . U_{j,t}^{CHP,G}, \forall j \in J, t \in T \tag{65}$$

$$U_{j,t}^{CHP,H} = \eta_j^{CHP,H} . U_{j,t}^{CHP,G}, \forall j \in J, t \in T \tag{66}$$

$$0 \le D_{j,t}^{CHP,G} \le P_{j,t}^{CHP,G} - \underline{P_{j,t}^{CHP,G}}, \forall j \in J, t \in T \tag{67}$$

$$D_{j,t}^{CHP,E} = \eta_j^{CHP,E} . D_{j,t}^{CHP,G}, \forall j \in J, t \in T \tag{68}$$

$$D_{j,t}^{CHP,H} = \eta_j^{CHP,H} . D_{j,t}^{CHP,G}, \forall j \in J, t \in T \tag{69}$$

CHPs have a slower response than the other electric resources and they are only able to provide 100% of their power within 60 s [38]. Constraint (70) limits the response of the CHPs to a fraction of its maximum power. This ensures that the CHPs can deliver the reserves traded in the secondary reserve market. Secondary reserve markets typically require full activations at fast response times (0–30 s).

$$U_{j,t}^{CHP,G}, D_{j,t}^{CHP,G} \le \mu^{CHP} . \overline{P_{j,t}^{CHP,G}}, \forall j \in J, t \in T \tag{70}$$

4. DSO sub-problems: multi-energy flow optimization models

In this section, we formulate the multi-energy flow models used by the DSOs to evaluate the network feasibility of the aggregator's offers. The DSOs use the delivery scenarios computed by the aggregator to check if the aggregator's offers violate or not the constraints of the multi-energy networks.

The role of the DSOs in this paper is to ensure multi-energy network security while opening up as much network capacity as possible for the aggregator to bid into the markets. The minimization of the operating costs of the DSOs, such as network losses, is not considered since the operation of the system is defined by the dispatch of the wholesale markets.

4.1. Time horizon and delivery scenarios

The optimisation problem is decomposed by time-step $t \in T$ and delivery scenarios $s \in \{E, U, D\}$ because there are no coupling constraints between different time-steps and delivery scenarios. In the next subsections, for the sake of readability, we drop the subscripts of time and delivery scenarios.

4.2. Electricity DSO sub-problem

Here, we formulate the optimization problem that the electricity DSO uses to evaluate the feasibility of the aggregator's offers.

4.2.1. Objective function

The objective function (71) minimizes the augmented Lagrangian penalty terms, which penalize electricity network violations.

$$min \sum_{n \in N^E} \left[\pi_n^E \left(P_n^E - \widehat{P}_n^E \right) + \frac{\rho}{2} \left(P_n^E - \widehat{P}_n^E \right)^2 \right] \tag{71}$$

4.2.2. Electricity network constraints

The electricity network is modelled using the non-convex formulation of the branch flow model [36,39]. Constraints (72)–(75) are the branch power flow equations. Constraints (76) and (77) set the limits of the square of the voltage and current magnitudes.

$$P_{m,n}^F = \frac{\widehat{P}_n^E}{SB} + \sum_{i:n \to i} P_{n,i}^F + r_{m,n} \ell_{m,n}, \forall (m,n) \in L^E \tag{72}$$

$$Q_{m,n}^F = Q_n^E + \sum_{i:n \to i} Q_{n,i}^F + x_{m,n} \ell_{m,n}, \forall (m,n) \in L^E \tag{73}$$

$$v_n = v_m - 2 \left(r_{m,n} P_{m,n}^F + x_{m,n} Q_{m,n}^F \right) + \left(r_{m,n}^2 + x_{m,n}^2 \right) \ell_{m,n}, \forall (m,n) \in L^E \tag{74}$$

$$\ell_{m,n} v_m = {P_{m,n}^F}^2 + {Q_{m,n}^F}^2, \forall (m,n) \in L^E \tag{75}$$

$$\underline{v_n} \le v_n \le \overline{v_n}, \forall n \in N^E \tag{76}$$

$$0 \le \ell_{m,n} \le \overline{\ell_{m,n}}, \forall (m,n) \in L^E \tag{77}$$

4.3. Gas DSO sub-problem

Here, we formulate the optimization problem that the gas DSO uses to evaluate the feasibility of the aggregator's offers.

4.3.1. Objective function

The objective function (78) minimizes the augmented Lagrangian penalty terms, which penalize gas network violations.

$$min \sum_{n \in N^G} \left[\pi_n^G \left(P_n^G - \widehat{P}_n^G \right) + \frac{\rho}{2} \left(P_n^G - \widehat{P}_n^G \right)^2 \right] \tag{78}$$

4.3.2. Gas network constraints

Constraints (79)–(80) limit gas production and nodal pressure.

$$\underline{P_i^g} \le P_i^g \le \overline{P_i^g}, \forall i \in N^g \tag{79}$$

$$\underline{P_n^G} \le p_i^G \le \overline{p_i^G}, \forall i \in N^G \tag{80}$$

Constraint (81) models the gas balance in each node. It considers that the gas that flows into a node also flows out of the node [13]. The factor c is assumed to be 11.4 ($1m^3 = 11.4kWh$) [40].

$$\frac{P_m^g}{c} - \frac{\widehat{P}_m^G}{c} + \sum_{n:m \to n} q_{m,n}^{Out} - \sum_{n:n \to m} q_{n,m}^{In} = 0, \forall m \in N^G \tag{81}$$

Constraint (82) defines the general equation for the steady-state gas flow [13]. It is assumed that the mass flow is constant in space, which means that the gas flowing into the pipe is equal to the gas flowing out of the pipe. K is calculated as in [40].

$$sgn\left(q_{m,n}\right) q_{m,n}^2 = K \left[\left(p_m^G \right)^2 - \left(p_n^G \right)^2 \right], \quad \forall (m,n) \in B^G \tag{82}$$

4.4. Heat DSO sub-problem

Here, we formulate the optimization problem that the heat DSO uses to evaluate the feasibility of the aggregator's offers.

4.4.1. Objective function

The objective function (83) minimizes the augmented Lagrangian penalty terms, which penalize heat network violations.

$$min \sum_{n \in N^H} \left[\pi_n^H \left(P_n^H - \widehat{P}_n^H \right) + \frac{\rho}{2} \left(P_n^H - \widehat{P}_n^H \right)^2 \right] \tag{83}$$

4.4.2. Heat network constraints

Heat networks consist of supply and return networks. Hydraulic and thermal optimizations are performed to calculate the mass flows and temperatures of pipes and nodes. In this model, it was assumed that the temperature of generator supply nodes and load return nodes are defined, as well as the heat power at all nodes, except the slack node.

4.4.2.1. Hydraulic model. Constraints (84) and (85) define the conservation of mass and pressure drop. Constraints (86)–(88) define the pressure and mass flow limits of pipelines and loads/generators [7]. The value of $k_{i,j}$ is calculated as in [14]. To relax the problem, the heat direction flow was initialized for each hour based on the algorithm developed in [9] and remained static for the rest of the iterations.

$$A.m = mq \tag{84}$$

$$p_i^H - p_j^H = k_{i,j}.m_{j,i}.\left|m_{j,i}\right|, \quad \forall (i,j) \in B^H \tag{85}$$

$$\underline{P_i^H} \le P_i^H \le \overline{p_i^H}, \forall i \in N^H \tag{86}$$

$$\underline{m_{i,j}} \le m_{i,j} \le \overline{m_{i,j}}, \forall (i,j) \in B^H \tag{87}$$

$$\underline{mq_i} \le mq_i \le \overline{mq_i}, \forall i \in N^H \tag{88}$$

4.4.2.2. Thermal model. The equations which relate to mass flow rate and temperature are the heat power equations, the temperature drop equations and conservation of energy. The heat power is defined by constraint (89) and the temperature limits of supply and outlet nodes are defined by constraints (90) and (91). The temperature drop equation, relating the temperature in the two ends of the pipe, is defined in constraint (92) and the temperature limits of pipelines are defined by constraints (93) and (94). The conservation of energy is presented in (95).

$$\widehat{P}_i^H = CP.mq_i.\left(\theta_i^S - \theta_i^{Ot}\right), \forall i \in N^H \tag{89}$$

$$\underline{\theta_i^S} \le \theta_i^S \le \overline{\theta_i^S}, \forall i \in N^H \tag{90}$$

$$\underline{\theta_i^{Ot}} \le \theta_i^{Ot} \le \overline{\theta_i^{Ot}}, \forall i \in N^H \tag{91}$$

$$\theta_{i,j}^{End} = \left(\theta_{i,j}^{Start} - \theta^{Amb}\right) e^{\frac{h.L}{CP.m_{i,j}}} + \theta^{Amb}, \forall (i,j) \in B^H \tag{92}$$

$$\underline{\theta_{i,j}} \le \theta_{i,j}^{End} \le \overline{\theta_{i,j}}, \forall (i,j) \in B^H \tag{93}$$

$$\underline{\theta_{i,j}} \le \theta_{i,j}^{Start} \le \overline{\theta_{i,j}}, \forall (i,j) \in B^H \tag{94}$$

$$\sum_j \left(\theta_j^{In}.m_j^{In} \right) = \theta_j^{Out}.\sum_j \left(m_j^{Out} \right), \forall j \in N^H \tag{95}$$

5. Test case

The proposed multi-energy and network-secure bidding strategy is evaluated using the microgrid from the University of Manchester [40], due to the unavailability of a suitable test case in the Iberian peninsula. The microgrid is characterized by electricity, gas, and heat networks, as illustrated in Fig. 3.

5.1. Network data

The data of the electricity, gas, and heat networks was sourced from [40]. This data includes the parameters of the networks, as well as the inflexible load profiles (electricity, gas, and heat) of the buildings. Regarding the electricity network, the bounds of the voltages were fixed at 0.9 and 1.1p.u., and the voltage in the slack bus 0 was fixed at 1p.u. Concerning the heat network, the mass flow limit was set at 40 kg/s, the supply temperature of generators was defined as 85 °C, the outlet temperature of each load was set at 70 °C and the ambient temperature of the ground was defined as 7 °C. At last, the limit of the gas network's pressure was set to 2 bar.

5.2. DMER data

The DMERs can be connected to the electricity, gas, and heat networks. The DMERs connected to the electricity network are PV systems, ESSs, HPs, and CHPs. The CHPs are also connected to the gas and heat networks. The district heating flexible loads are connected to the heat network.

The PV systems are connected to the electricity nodes 14, 19 and 20 and buildings 3, 7, 12, 14, 24 and 34. The peak power of the PV systems ranges from 750 to 1500 kW. Real PV profiles were used in the simulations performed.

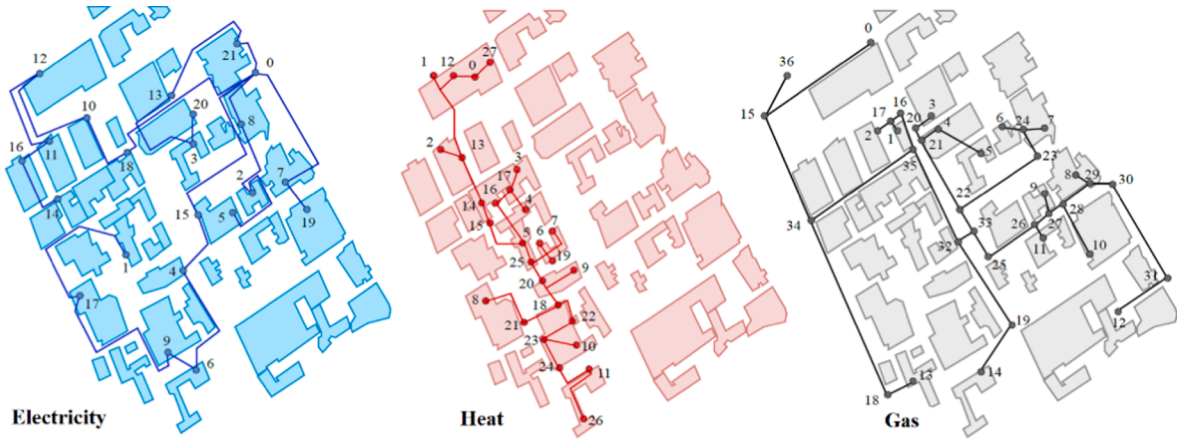

Fig. 3. Electricity, heat and gas networks of the study case [40].

The ESSs are connected to the electricity nodes 5, 9, 15, 18 and 20 and buildings 4, 8, 11, 12, 14, 19, 24, 31, 33 and 34. The parameters of the ESSs are 250 kWh of capacity, 0.9 of efficiency, and 100 kW of maximum power for charging and discharging.

The HPs are connected to the electricity nodes 2, 5, 15, 19 and 20 and buildings 8, 11, 22, 34 and 39. Its parameters are 3.45 of COP, and 750 kW of maximum electric power.

The CHPs are connected to the electricity nodes 6 and 12, gas nodes 0 and 14 and heat nodes 26 and 27. The parameters of the CHPs are 10 MW of maximum gas power, 0.35 of electricity efficiency, 0.45 of heat efficiency, and 1/3 of ramp rate μ^{CHP}.

The district heating flexible loads are connected to the heat nodes 2, 5 and 22 and buildings 2, 13, 15, 25 and 32. The only parameter of the district heating flexible loads is 750 kW of maximum heating power.

The buildings connected to the HPs and district heating flexible loads are characterized by β of 0.97 and R of 0.081 °C/kWh. The comfort range of the users was set to [19,23] °C between 7 h and 18 h, and [16,26] °C for the rest of the day. Real outdoor temperature profiles were used in the simulations performed.

5.3. Market data

The electricity market data includes forecasts of energy price, secondary reserve price, upward and downward tertiary reserve prices, ratios of upward and downward mobilizations, as illustrated in Fig. 4. This information was sourced from references [41,42].

The gas market data includes forecasts of gas price (22.96 €/MWh) and gas imbalance prices (22.26€/MWh for both directions) [43]. The carbon market includes the price of CO2 emission allowances (25 €/tCO2), the free allowances (2.8 tCO2), and the conversion factor (0.2 tCO2/MWh).

6. Results

In this section, we discuss and compare the results computed by three different bidding strategies. The bidding strategies are the following:

- Multi-energy and network-free (M−NF) strategy: under this strategy, an aggregator manages DMERs and computes bids without considering the constraints of the energy networks;
- Single-energy and network-free (S-NF) strategy: under this strategy, an aggregator only manages single energy-vector resources and computes bids without considering the constraints of the energy networks. This strategy was evaluated using two aggregators, one with only electricity resources, and another with only gas resources;
- Multi-energy and network-secure (M−NS) strategy: under this fully integrated approach, an aggregator manages DMERs and computes network-secure bids.

In subsection 6.1, the performance of the mentioned bidding strategies is compared and discussed, whereas in subsection 6.2, two sensibility studies are performed using the M−NF strategy.

6.1. Performance analysis of the bidding strategies

This section discusses the results obtained for each strategy focusing on the placement of aggregator's bids (6.1.1), the disaggregated band bids deployed per resource (6.1.2), the impacts of the multi-energy bids in the energy networks (6.1.3), the economic performance (6.1.4), the CO2 emissions (6.1.5) and finally, the computational performance (6.1.6).

6.1.1. Optimized multi-energy bids

Fig. 5 presents the electricity (energy and secondary reserve band),

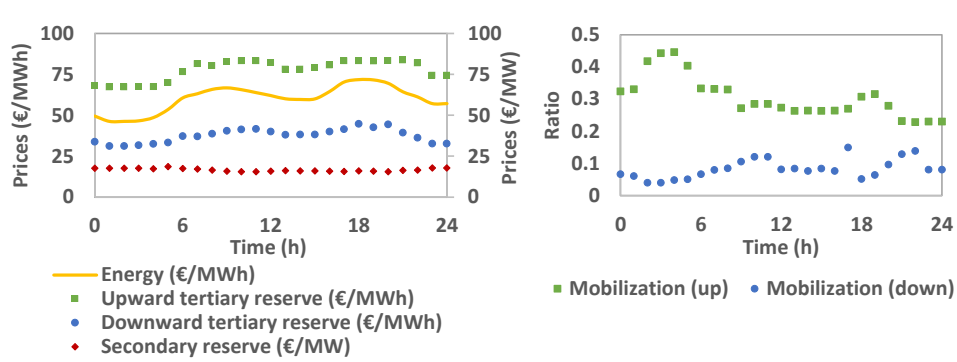

Fig. 4. Electricity market data.

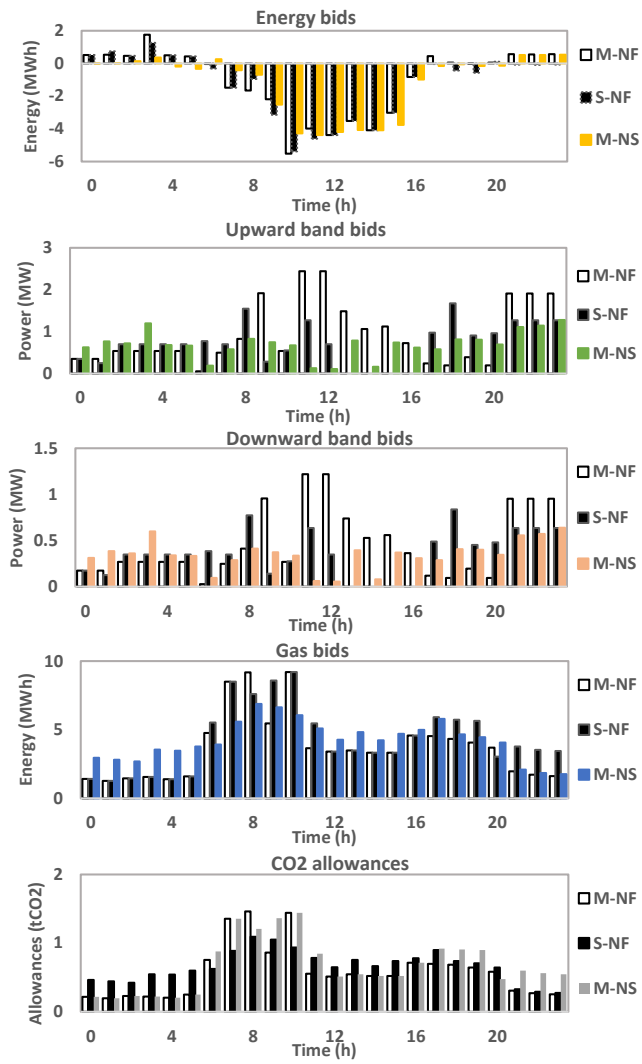

Fig. 5. Aggregator's bids.

gas, and CO2 allowance bids submitted by the aggregator(s) to the day-ahead markets, under the M−NF, S-NF, and M−NS strategies. It is important to note that gas and CO2 bids are presented in the market as daily bids and not hourly bids. The hourly disaggregation presented is only for analysis purposes.

The three bidding strategies present similar placement behaviors in the day-ahead energy market (electricity). Demand (positive values) and supply (negative values) bids are mainly influenced by PV production, prices, and heat requirements. The aggregator places most of the supply bids during the period of forecasted PV generation (i.e., during day-light time). Under M−NF and S-NF strategies, the aggregator placed a high quantity of demand bids at 3 h to benefit from lower prices to heat the buildings.

The three bidding strategies also present some placement similarities in the day-ahead gas market. The gas bids are mainly influenced by prices and heat requirements. Most of the gas was bought to supply the CHPs, which generate heat to satisfy heat load requirements of the prosumers connected to the heat network. The heat load requirements are stricter between 7 h and 18 h, which leads the aggregator to buy more gas in the market. During this period, the bids end up following the electricity energy prices as it can profit from the injection of electricity from the CHPs and higher prices. From 0 h to 5 h and from 21 h forward, the gas bids do not change much, which can suggest that at these hours, the aggregator is only fulfilling gas loads and heat load requirements expected from the CHPs. As the CO2 allowances bids are directly related

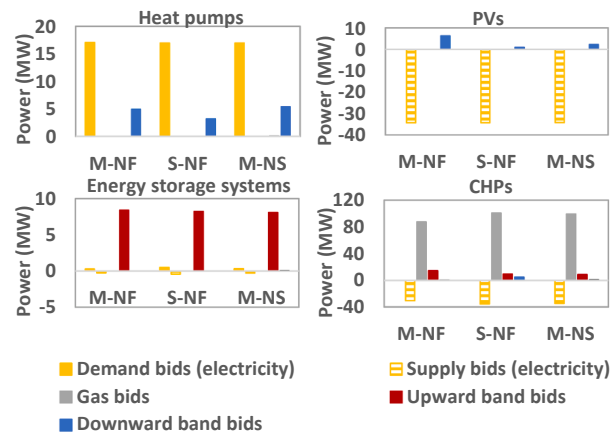

Fig. 6. Disaggregation of the electricity (energy and secondary reserve band) and gas bids by DMER.

to the CHP production, their behavior is very similar to the gas bids.

M−NF and S-NF strategies presented more electricity and gas bids to the day-ahead markets than the M−NS strategy. The electricity bids include energy and secondary reserve bids in both downward and upward directions. The difference of bids indicates that M−NF and S-NF strategies may have encountered scenarios with a large injection of electricity (from PV and CHPs) which caused violations of the electricity network constraints. To mitigate this problem, the M−NS strategy reduced the quantities of the electricity and gas bids.

In addition, M−NF and S-NF strategies present very different placements of secondary reserve bids in both upward and downward directions. This is related to the fact that the M−NF strategy has more sources of flexibility, which allows it to offer higher upward and downward bids.

6.1.2. *Disaggregation of the aggregator's bids per DMER*

Fig. 6 presents the disaggregation of electricity and gas bids per DMER. Comparing M−NF and S-NF strategies, the energy bids are similar for all the DMERs with a small difference of 4.7 MWh for the CHPs. The electrical DMERs (HPs, PVs, and ESSs) provided a total of 8.4 MW and 11.2 MW of upward and downward bands under the M−NF strategy.

In the S-NF strategy, there is a slight decrease in the provision of the upward band bid (-0.2 MW) and a great decrease in the provision of downward band bid (-7.1 MW) by electricity DMERs. This occurs because the electricity aggregator in the S-NF strategy must comply with constraint (19) and can only use electricity DMERs. This way, the aggregator is still able to maximize the provision of upward band by electricity DMERs, but it highly decreases its capability in providing downward band. In relation to gas DMERs, under the S-NF strategy, it is possible to observe a decrease in the CHPs capacity of providing upward band bid (-4.9 MW) as they are constrained by constraint (19) and prosumers' constraints. These results allow concluding that a mix of electric and gas DMERs can optimize the capability of each resource in

Table 1
Voltage results for the electricity network.

		Energy scenario	Upward scenario	Downward scenario
Number violations	**M−NF**	6	11	1
	S-NF	6	8	3
	M−NS	0	0	0
Maximum voltage (p.u.)	**M−NF**	1.112	1.125	1.101
	S-NF	1.118	1.126	1.118
	M−NS	1.099	1.100	1.099

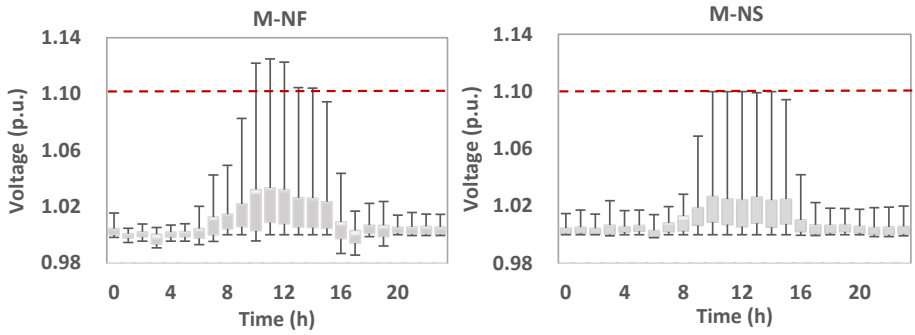

Fig. 7. Voltages results for the upward scenario.

Table 2
Mass flow results for the district heating network.

		Energy scenario	Upward scenario	Downward scenario
Number violations	**M−NF**	2	4	1
	S-NF	2	8	2
	M−NS	0	0	0
Maximum mass flow (kg/s)	**M−NF**	42.8	42.8	42.16
	S-NF	45.9	45.9	45.9
	M−NS	30.6	36.1	30.6

offering reserve band bids.

Comparing M−NF and M−NS strategies, the consumption and supply of electricity are similar for all DMERs except for CHPs, which had an increase in electricity supply (+4.1 MW). The HPs had an increase in downward band while the PVs had a decrease. The ESSs had a similar provision of upward band and the CHPs decreased it. In the overall, the M−NS strategy provided the lowest reserve band to counteract the network problems encountered under the M−NF strategy.

6.1.3. *Multi-energy networks*

In this section, we evaluate the feasibility of the aggregator's offers in the electricity, gas, and heat networks. Regarding the electricity network, the voltage results for each strategy are presented in Table 1 and Fig. 7. We can observe that M−NF and S-NF strategies generated overvoltage problems, which surpassed the limit of 1.1. The maximum values of 1.125 and 1.126p.u were observed under the M−NF and S-NF strategies for the upward activation scenario. On the contrary, the M−NS strategy did not encounter any voltage problem. It remained at the upper voltage limit. This proves that the M−NS strategy computes network-secure bids from the electricity network perspective.

The district heating results are presented in Table 2 and Fig. 8. We can observe that violations of the mass flow occurred in the NF strategies, especially in the upward scenario. Contrarily, the M−NS strategy was able to calculate bids without any network violation. In Fig. 8, we can observe that the mass flows were almost at their limits but never surpassing them. On the other hand, under the M−NF strategy, the mass flows violated the limits of the heat network between 6 h and 9 h.

When calculating the bids of the M−NF strategy, the heat losses were not considered as it was assumed that the CHP generation had to be equal to the heat consumption from the district heating. This way, the actual heat to be produced by CHPs will be higher than the one calculated, which will incur in higher costs. For example, in the M−NF strategy, the total heat load is 41.2 MW for the entire day. The necessary generation to fulfill this load is 42.6 MW, which represents an increase of 1.4 MW (4%). Thus, part of the energy to be bought or sold was not duly distributed and optimized. This problem does not occur in the M−NS strategy, adding another advantage to it.

In relation to the gas network, no violations were observed under any bidding strategy. Nonetheless, if any problem had occurred under the NF strategies, the M−NS strategy would have avoided the problem.

6.1.4. *Economic performance*

Table 3 presents the cumulative costs obtained for the three bidding strategies. Positive values represent costs and negative values represent income. The costs of the S-NF strategy are the sum of the costs of aggregators 1 and 2. The results in Table 3 show that the M−NF strategy produced the most profitable outcome, followed by M−NS and S-NF strategies. The M−NF strategy outperformed the S-NF strategy with 89%

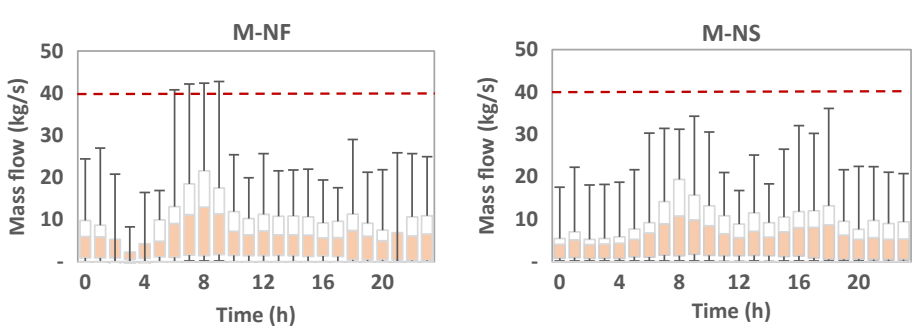

Fig. 8. Mass flows for the upward scenarios.

Table 3
Costs of each strategy.

	M−NF	S-NF	M−NS
Electricity – energy (€)	− 1 583	− 1 883	−1 660
Gas - energy (€)	2 290	2 492	2 351
Electricity – secondary reserve (€)	− 1 014	− 824	−902
Carbon (€)	322	356	332
Total (€)	14	142	112

lower costs, which allows us to conclude that a multi-energy aggregator exploits better the flexibility of DMERs than single-energy aggregators. Comparing the results of M−NF and M−NS strategies, we conclude that the M−NF strategy is more profitable since it is not limited by the constraints of the electricity, gas, and heat networks, which prevents the aggregator from using the maximum flexibility of the DMERs.

The M−NF strategy may produce bidding solutions with lower costs. However, these solutions may be network-infeasible, as described in section 6.1.3. These network infeasibilities will end up significantly increasing the costs of the aggregator in real-time since he will not be able to deliver the services traded in the day-ahead markets, due to network violations.

6.1.5. Carbon allowances

Table 4 presents the CO2 allowances bought by the aggregator due to the electricity and heat generated by CHPs. The results show that the M−NF strategy produces the lowest total of CO2 allowances, followed by M−NS and S-NF strategies. Moreover, the free allowances were not sufficient to fulfill the needs and only covered 30.9% to 35.6% of the total needs.

6.1.6. Computational performance

The optimization sub-problems of the bidding strategies were implemented in Python 3.7 and solved in an Intel® Core™ i5.8265U CPU @ at 1.6 GHz with 8 GB RAM. The aggregator sub-problem is a mixed-integer quadratic program and was solved by the *IBM CPLEX v12.9.0* optimizer. The sub-problem of each DSO is a non-linear program and was solved by the *IPOPT v3.11.1* optimizer.

Table 5 presents the execution times and the sizes of the bidding optimization problems, divided by sub-problems. The DSOs' sub-problems result from the decomposition of the multi-temporal and multi-scenario problems into smaller sub-problems, as described in section 4.1. The total size of the M−NS results from the sum of the aggregator sub-problem to all DSOs' sub-problems, representing the equivalent size of the centralized problem. The total time is the execution time of the ADMM.

The optimization bidding times of the M−NF and S-NF strategies were 0.58 s and 0.51 s (max (0.51, 0.35)), respectively. In relation to the M−NS strategy, if we run in parallel and do not consider the communication times between the aggregator, DSOs and the independent platform, an iteration can be run in 1.52 s (0.51 + max (0.05, 0.1, 1.01)). Considering that the ADMM algorithm runs in 157 iterations, it would take 239 s to run the M−NS strategy. It is possible to conclude that the M−NF and S-NF strategies were faster than the M−NS strategy. Nonetheless, any of the three strategies present suitable execution times for the timelines of the electricity, gas, and carbon markets.

Table 4
CO2 allowances of each strategy.

	M−NF	S-NF	M−NS
Electricity (tCO2)	6.1	7.1	6.4
Heat (tCO2)	7.9	9.1	8.3
Free allowances (tCO2)	2.8	2.8	2.8
Total (tCO2)	11.2	13.3	11.9

Table 5
Size and execution time of the bidding optimization strategies.

Strategy	Sub-problems	N° of variables	N° of constraints	Time (s)
M−NF	**Aggregator**	40 619	64 633	0.58
S-NF	**Aggregator 1**	37 163	56 401	0.51
	Aggregator 2	30 313	33 097	0.35
M−NS	**Aggregator**	40 619	64 585	0.51
	Electricity DSO	10 848	20 496	0.05
	Gas DSO	14 064	31 488	0.10
	Heat DSO	38 448	141 048	1.01
	Total	103 979	257 617	239

6.1.6.1. Convergence of the ADMM under the M−NS strategy. The literature has been proving that the ADMM is globally convergent for convex problems [37]. Nonetheless, recent works [22,44] also show that the ADMM converges for many non-convex problems, as demonstrated here by Fig. 9. Both primal and dual residuals converged to the stop criteria at iteration 157. The absolute tolerance ϵ^{Abs} was set to 0.0001 which corresponds to a stop criterion of 0.007 kW in the case of the primal residual. After iteration 157, it was decided to run the ADMM until iteration 250 in order to check the variation of the aggregator's cost. We observed almost no variation of the aggregator's cost after iteration 157 (0.06% variation), which demonstrates that the ADMM converged to a stationary solution.

The choice of the absolute tolerance ϵ^{Abs} impacts the convergence of the ADMM, as illustrated in Fig. 10. We can observe that the number of iterations increases linearly with the reduction of the absolute tolerances, which impacts similarly the computational times. It is worth mentioning here that the computational time is quite fast even for the most conservative absolute tolerance of 0.0001.

6.1.6.2. Centralized versus distributed formulation for the M−NS strategy. The centralized formulation of the M−NS strategy assumes the form of a mixed-integer non-linear problem. As reported in Table 5, this problem has 103 979 variables and 257 617 constraints. Solving such a large-scale mixed-integer non-linear problem in a reasonable time was not possible using state-of-the-art solvers on a computer with 8 GB RAM. To solve this optimization problem in a reasonable time, it would be necessary to set a time limit and the mixed-integer non-linear solvers would only compute a sub-optimal solution, when possible. The application of the ADMM made it possible to solve the problem in reasonable computational times. In addition to this computational advantage, the ADMM allows the aggregator and DSOs to preserve their data privacy and ensure a clear separation of their roles by solving the problem in a distributed manner.

6.2. Sensibility studies

In this section, two sensibility studies are presented related to the economic value of the CHPs' ramp-rate (6.2.1) and the CO2 emissions price (6.2.2), considering the M−NF strategy.

6.2.1. Economic value of the CHPs' ramp rate

As previously stated, the CHPs have a slow ramp-rate (100% of its capacity per minute) compared to the other DMERs, such as PVs, HPs, and ESSs, which can deploy their full capacity in a few seconds. This affects the participation in secondary reserve markets because energy resources must fully deliver the service in 30 s. According to the market rules, there is a range between 0 and 30 s for the aggregator to respond to the automatic generation control (AGC) signal used to activate secondary reserve. However, there is a trade-off between a fast response and the maximum power of the CHPs. A fast response reduces the maximum power of the CHPs. Therefore, the aggregator must select the most suitable response time for the CHPs. In this section, we discuss the impact of the response time on the costs of the aggregator.

Table 6 presents the aggregator's costs when deciding to participate

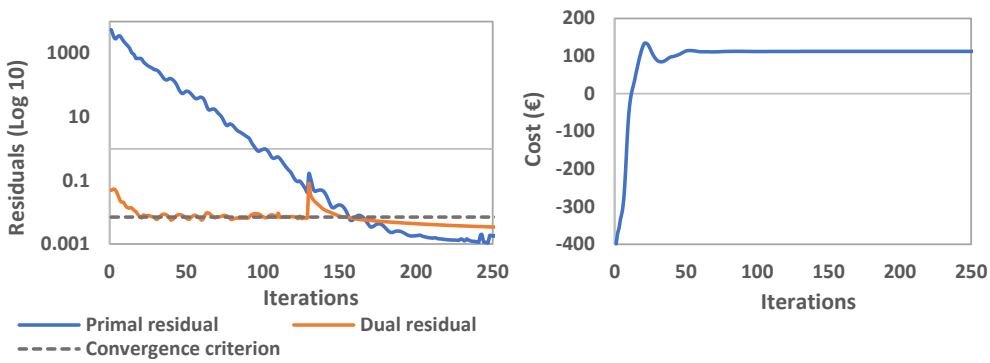

Fig. 9. Residuals (left) and aggregator's costs (right).

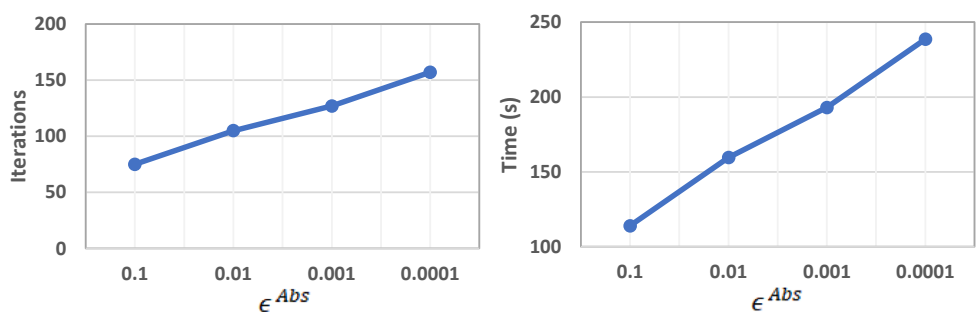

Fig. 10. Number of iterations and computational times across different absolute tolerances.

Table 6
Aggregator's costs for different response times of the CHPs.

Response time of the CHP (s)	5 s	10 s	15 s	20 s	25 s	30 s
CHPs maximum power (kW)	**833**	**1667**	**2500**	**3333**	**4167**	**5000**
Electricity – energy (€)	−1584	−1577	−1600	−1583	−1583	−1583
Gas - energy (€)	2238	2263	2304	2290	2290	2290
Electricity – secondary reserve (€)	857	943	1008	1014	1014	1014
Carbon (€)	312	317	324	322	322	322
Total (€)	109	60	20	14	14	14

Table 7
Aggregator costs considering different CO2 prices.

Price of CO2 (€/tCO2)	0	25	100	200	300	400	500
Total cost (€)	−308	14	976	2245	3402	4510	5619

in the day-ahead markets with different response times for the CHPs. The results show that slower response times produce lower costs as the maximum power of the CHPs increases. Comparing the cases with response times of 20 s and 5 s, the costs can be 87% lower. Nonetheless, when the response time is equal or higher than 20 s, there are no economic benefits. This way, it is important that the aggregator analyses the best response time to adopt in its bidding strategy to follow the AGC signal when there are resources that present a slower response than others, as is the case of CHPs. Furthermore, the response time not only affects the participation in the secondary reserve market but also the participation in the energy (electricity), gas, and carbon markets, as well as the strategy of the aggregator.

6.2.2. *Impact of the carbon price in the aggregator performance*

The results of Table 7 show that increasing the CO2 price rises the aggregator's costs. If we compare a CO2 price of 0€/tCO2 to 25€/tCO2 (used in the previous sections), we can observe that the net cost increases from −308€ to 14€, representing a 105% rise. On the other hand, the increase of the CO2 price did not have the same impact on the energy and band bids, as shown in Fig. 11. The energy bids of the CHPs decreased from −30.8 MW to −30.6 MW. The upward bids remained the same for both cases with 14.3 MW, and the downward bids decreased from 0.3 MW to 0.1 MW. Therefore, CO2 prices have a significant impact on the aggregator's costs, but they do not significantly impact the operation of the CHPs.

To have a significant impact on the bidding behavior of the CHPs and respective CO2 emissions, the price would have to increase to more than 200€/tCO2. This is possible to observe in Fig. 11, as CHPs' upward band decreased from 14.2 MW to 0 MW. This decrease not only significantly impacts the aggregators' total upward bids (63%), but also the downward bids (63% as well), as they must comply with constraint (19). The energy bids of the CHPs were not so affected, as they must satisfy the minimum requirements of the district heating loads.

From another point of view, it is also possible to conclude that carbon markets may have a negative impact on the provision of secondary reserve since the band bids offered by the aggregator decreased with higher prices. This only occurs if the DMERs used for providing these reserves are affected by the carbon market. Nonetheless, the increase of the CO2 prices rises the operating costs of the CHPs, which may incentivize the adoption of only electricity resources by the aggregator.

7. Conclusions

This paper presents a network-secure bidding strategy for multi-energy aggregators to participate in day-ahead electricity (energy and reserves), gas and carbon markets. Using a distributed approach based on the ADMM algorithm, the aggregator negotiates with the electricity, gas and heat distribution system operators to compute network-secure

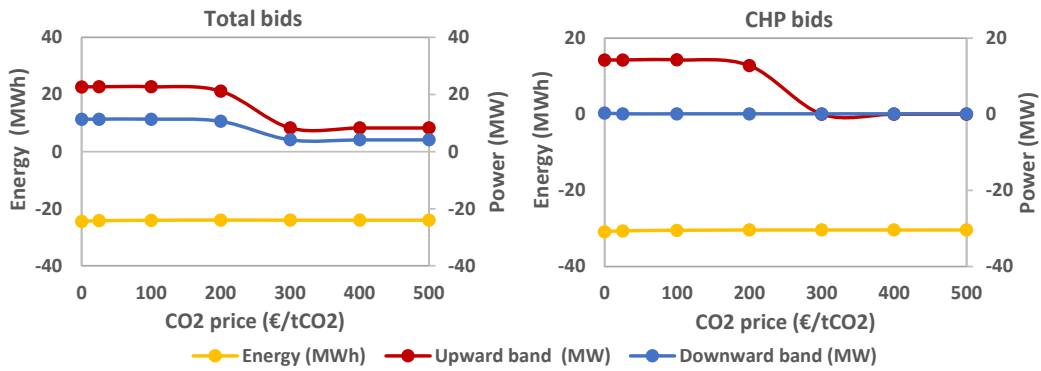

Fig. 11. Impact on electricity (energy and reserve) bids considering different CO2 prices.

and multi-energy bids. This approach allows aggregators to preserve their data privacy.

The proposed bidding strategy was benchmarked against two other strategies. The numerical results of these comparisons yielded three main findings. The first one shows that the proposed strategy counteracts all the operating problems of the electricity, heat and gas networks and provides network-secure bids. This avoids the situation of significantly increasing aggregator's costs in real-time as he would not be able to deliver the services offered in the day-ahead markets due to network violations. The second finding revealed that the aggregator's costs of trading energy, gas and carbon allowances can decrease up to 89% when considering a strategy that jointly optimizes multi-energy systems. Finally, the third one confirmed that the execution time of this strategy is well suited for the timelines of the electricity, gas, and carbon markets.

In addition, two sensibility studies were also performed. In the first one, the economic impact of the combined heat and power resources' response time to the automatic generation control signal was evaluated. We found that the aggregator's costs may decrease up to 87% when considering slower response times. In the second study, the impact of carbon prices on the economic performance of the aggregator was assessed. We found that the costs of the aggregator increase with the increase of the carbon prices, but the bids only begin to change significantly when prices rise above 200€/tCO2.

Future work consists of studying the impact of uncertainty in the network-secure bidding problem. Modelling uncertainty through stochastic optimization may reduce the settlement cost of the multi-energy aggregator (by 2–3% in [21]), but it may also increase the execution time beyond suitable values. We also expect to extend the DSO subproblems to consider the minimization of their operating costs (e.g., network losses). Moreover, it is expected the demonstration of the proposed approach in a real-world setting, under the scope of the ATTEST project.

CRediT authorship contribution statement

António Coelho: Conceptualization, Methodology, Formal analysis, Investigation, Software, Writing – original draft, Writing – review & editing. **José Iria:** Conceptualization, Methodology, Formal analysis, Writing – original draft, Writing – review & editing, Supervision, Funding acquisition. **Filipe Soares:** Conceptualization, Supervision, Writing – original draft, Writing – review & editing, Funding acquisition, Project manager.

Declaration of Competing Interest

The authors declare that they have no known competing financial interests or personal relationships that could have appeared to influence the work reported in this paper.

Acknowledgments

The research leading to this work has been carried out as part of the ATTEST project. The ATTEST project was funded by the European Union's Horizon 2020 research and innovation programme under grant agreement No 864298. In addition to the support of the ATTEST project, the work of António Coelho was financed by FCT—Fundação para a Ciência e a Tecnologia (Portuguese Foundation for Science and Technology) through the grant PD/BD/142811/2018.

The authors would also like to thank Eduardo Alejandro Martinez Cesena from the University of Manchester for providing and clarifying the data of the test case used in this work.

References

[1] Nations U. Paris Agreement. 2015.
[2] European Commission. Communication from the Comission to the European Parliment, the Council, the European Economic and Social Committee and the Committee of the Regions. 2020.
[3] European Comission. EU ETS Handbook. 2015.
[4] Zhang Y, He Y, Yan M, Guo C, Ding Y. Linearized Stochastic Scheduling of Interconnected Energy Hubs Considering Integrated Demand Response and Wind Uncertainty. Energies 2018;11:2448. https://doi.org/10.3390/en11092448.
[5] Wang C, Wei W, Wang J, Bi T. Convex optimization based adjustable robust dispatch for integrated electric-gas systems considering gas delivery priority. Appl Energy 2019;239:70–82. https://doi.org/10.1016/j.apenergy.2019.01.121.
[6] Bai L, Li F, Cui H, Jiang T, Sun H, Zhu J. Interval optimization based operating strategy for gas-electricity integrated energy systems considering demand response and wind uncertainty. Appl Energy 2016;167:270–9. https://doi.org/10.1016/j.apenergy.2015.10.119.
[7] Liu X, Wu J, Jenkins N, Bagdanavicius A. Combined analysis of electricity and heat networks. Appl Energy 2016;162:1238–50. https://doi.org/10.1016/j.apenergy.2015.01.102.
[8] Li Z, Wu W, Shahidehpour M, Wang J, Zhang B. Combined heat and power dispatch considering pipeline energy storage of district heating network. IEEE Trans Sustain Energy 2016;7:12–22. https://doi.org/10.1109/TSTE.2015.2467383.
[9] Cao Y, Wei W, Wu L, Mei S, Shahidehpour M, Li Z. Decentralized Operation of Interdependent Power Distribution Network and District Heating Network: A Market-Driven Approach. IEEE Trans Smart Grid 2018;10:5374–85. https://doi.org/10.1109/TSG.2018.2880909.
[10] Cesena EAM, Mancarella P. Energy Systems Integration in Smart Districts: Robust Optimisation of Multi-Energy Flows in Integrated Electricity, Heat and Gas Networks. IEEE Trans Smart Grid 2018:1. https://doi.org/10.1109/TSG.2018.2828146.
[11] Liu X, Mancarella P. Modelling, assessment and Sankey diagrams of integrated electricity-heat-gas networks in multi-vector district energy systems. Appl Energy 2016;167:336–52. https://doi.org/10.1016/j.apenergy.2015.08.089.
[12] Shabanpour-Haghighi A, Seifi AR. Simultaneous integrated optimal energy flow of electricity, gas, and heat. Energy Convers Manag 2015. https://doi.org/10.1016/j.enconman.2015.06.002.
[13] Correa-Posada CM, Gas S-M, Optimization N. A comparison of Piecewise Linear Models. Lect Notes Comput Vis Biomech 2012;5:133–59. https://doi.org/10.1007/978-94-007-4552-0_6.
[14] Pirouti M. Modelling and analysis of a district heating network 2013:121.
[15] Iria J, Heleno M, Candoso G. Optimal sizing and placement of energy storage systems and on-load tap changer transformers in distribution networks. Appl Energy 2019;250:1147–57. https://doi.org/10.1016/j.apenergy.2019.04.120.
[16] Luo L, Wu Z, Gu W, Huang H, Gao S, Han J. Coordinated allocation of distributed generation resources and electric vehicle charging stations in distribution systems

with vehicle-to-grid interaction. Energy 2020;192:116631. https://doi.org/10.1016/j.energy.2019.116631.
[17] Bessa RJ, Matos MA. Optimization Models for EV Aggregator Participation in a Manual Reserve Market. IEEE Trans Power Syst 2013;28:3085–95. https://doi.org/10.1109/TPWRS.2012.2233222.
[18] Bessa RJ, Matos MA. Optimization models for an EV aggregator selling secondary reserve in the electricity market. Electr Power Syst Res 2014;106:36–50. https://doi.org/10.1016/j.epsr.2013.08.006.
[19] Iria J, Soares F, Matos M. Optimal bidding strategy for an aggregator of prosumers in energy and secondary reserve markets. Appl Energy 2019;238:1361–72. https://doi.org/10.1016/j.apenergy.2019.01.191.
[20] Iria JP, Soares FJ, Matos MA. Trading Small Prosumers Flexibility in the Energy and Tertiary Reserve Markets. IEEE Trans Smart Grid 2018:1. https://doi.org/10.1109/TSG.2018.2797001.
[21] Iria J, Soares F, Matos M. Optimal supply and demand bidding strategy for an aggregator of small prosumers. Appl Energy 2018;213:658–69. https://doi.org/10.1016/j.apenergy.2017.09.002.
[22] Iria J, Scott P, Attarha A. Network-constrained bidding optimization strategy for aggregators of prosumers. Energy 2020;207:118266. https://doi.org/10.1016/j.energy.2020.118266.
[23] Attarha A, Scott P, Thiébaux S. Network-aware co-optimisation of residential DER in energy and FCAS markets. Electr Power Syst Res 2020;189:106730. https://doi.org/10.1016/j.epsr.2020.106730.
[24] Wang H, Riaz S, Mancarella P. Integrated techno-economic modeling, flexibility analysis, and business case assessment of an urban virtual power plant with multi-market co-optimization. Appl Energy 2020;259:114142. https://doi.org/10.1016/j.apenergy.2019.114142.
[25] Yazdani-Damavandi M, Neyestani N, Shafie-khah M, Contreras J, Catalao JPS. Strategic Behavior of Multi-Energy Players in Electricity Markets as Aggregators of Demand Side Resources Using a Bi-Level Approach. IEEE Trans Power Syst 2018;33:397–411. https://doi.org/10.1109/TPWRS.2017.2688344.
[26] Neyestani N, Yazdani-Damavandi M, Shafie-khah M, Chicco G, Catalao JPS. Stochastic Modeling of Multi-Energy Carrier Dependencies in Smart Local Networks with Distributed Energy Resources. IEEE Trans Smart Grid 2015;6:1748–62. https://doi.org/10.1109/TSG.2015.2423552.
[27] Yazdani-Damavandi M, Neyestani N, Chicco G, Shafie-Khah M, Catalão JPS. Aggregation of Distributed Energy Resources under the Concept of Multienergy Players in Local Energy Systems. IEEE Trans Sustain Energy 2017;8:1679–93. https://doi.org/10.1109/TSTE.2017.2701836.
[28] Naughton J, Wang H, Riaz S, Cantoni M, Mancarella P. Optimization of multi-energy virtual power plants for providing multiple market and local network services. Electr Power Syst Res 2020;189:106775. https://doi.org/10.1016/j.epsr.2020.106775.
[29] Steriotis K, Smpoukis K, Efthymiopoulos N, Tsaousoglou G, Makris P, Varvarigos E (Manos) M. Strategic and network-aware bidding policy for electric utilities through the optimal orchestration of a virtual and heterogeneous flexibility assets' portfolio. Electr Power Syst Res 2020;184:106302. https://doi.org/10.1016/j.epsr.2020.106302.
[30] Spot E, Pool N, OMIE, OPCOM, GME, OTE, et al. EUPHEMIA Public Description - PCR Market Coupling Algorithm. 2016.
[31] Lam LH, Ilea V, Bovo C. European day-ahead electricity market coupling: Discussion, modeling, and case study. Electr Power Syst Res 2018;155:80–92. https://doi.org/10.1016/j.epsr.2017.10.003.
[32] Pillay A, Prabhakar Karthikeyan S, Kothari DP. Congestion management in power systems - A review. Int J Electr Power Energy Syst 2015;70:83–90. https://doi.org/10.1016/j.ijepes.2015.01.022.
[33] Entidade Reguladora dos Serviços Energéticos (ERSE). Manual of procedures for the management of the power system [in Portuguese]. vol. Abril. 2020.
[34] Entidade Reguladora dos Serviços Energéticos (ERSE). Manual of procedures for the access to natural gas infrastructures [in Portuguese]. 2017.
[35] European Commission. Commission Delegated Regulation (EU) 2019/331. 2018.
[36] Baran ME, Wu FF. Optimal capacitor placement on radial distribution systems. IEEE Trans Power Deliv 1989;4:725–34. https://doi.org/10.1109/61.19265.
[37] Boyd S, Parikh N, Chu E, Eckstein J, Boyd S, Parikh N, et al. Distributed Optimization and Statistical Learning via the Alternating Direction Method of Multipliers. Found Trends R Mach Learn 2010;3:1–122. https://doi.org/10.1561/2200000016.
[38] Energy W. Energy Solutions. 2020.
[39] Baran M, Wu FF. Optimal sizing of capacitors placed on a radial distribution system. IEEE Trans Power Deliv 1989;4:735–43. https://doi.org/10.1109/61.19266.
[40] Cesena EAM, Loukarakis E, Good N, Mancarella P. Integrated Electricity-Heat-Gas Systems: Techno-Economic Modeling, Optimization, and Application to Multienergy Districts. Proc IEEE 2020:1–19. https://doi.org/10.1109/jproc.2020.2989382.
[41] ENTSO-E. Transparency Platform n.d. https://transparency.entsoe.eu/dashboard/show (accessed November 24, 2020).
[42] REN. SIMEE - Mercado Diário e Intradiário n.d. https://www.mercado.ren.pt/PT/Electr/InfoMercado/InfOp/MercOmel/Paginas/default.aspx (accessed November 24, 2020).
[43] Gás M-MI de. Preços diários da MIBGAS n.d. https://www.mibgas.es/pt/market-results (accessed November 24, 2020).
[44] Rodriguez JS, Nicholson B, Laird C, Zavala VM. Benchmarking ADMM in nonconvex NLPs. Comput Chem Eng 2018;119:315–25. https://doi.org/10.1016/j.compchemeng.2018.08.036.
[45] Hu J, Yang G, Bindner HW, Xue Y. Application of Network-Constrained Transactive Control to Electric Vehicle Charging for Secure Grid Operation. IEEE Trans Sustain Energy 2017;8:505–15. https://doi.org/10.1109/TSTE.2016.2608840.